D/H ratio during the northern polar summer and what the Phoenix mission might measure

David Fisher,[1] Robert Novak,[2] and Michael J. Mumma[3]

Received 25 July 2007; revised 6 March 2008; accepted 6 June 2008; published 23 September 2008.

[1] The Phoenix polar mission will land close to 68°N, 233°E in May 2008 at Ls ~ 75 and operate 90 sols until Ls ~ 125 with possible extension to Ls ~ 142. Phoenix Meteorology (MET), Thermal and Evolved Gas Analyzer (TEGA) and Microscopy, Electrochemistry and Conductivity Analyzer (MECA) instrument packages will measure the air's temperature, water vapor concentration, ice crystal concentration and the water's stable isotope ratio D/H, and the D/H for the uppermost ground ice. This paper summarizes what is known about the seasonal cycle of atmospheric D/H and makes a theoretical connection between the atmospheric ratio and that expected from the ground ice that Phoenix will sample. A simple mixed cloud stable isotope model is used to show that the seasonal progress of D/H in the polar region cannot be used alone. It is argued that the seasonal cycle in D/H is explained by their being an interplay between multilatitudinal sources or reservoirs that have a range of reservoir D/H values. These reservoirs have different sizes and seasonal response times so that they release their water contributions at different times of the spring and summer and together explain most of the seasonal D/H observed by Mumma et al. (2003) and Novak et al. (2005). Phoenix observations from its high-latitude vantage point during the summer and fall will add some atmospheric D/H values, temperature, water vapor concentration, and ice cloudiness data points that will constrain the various theoretical possibilities. The D/H of the ice recovered by Phoenix from the surface of the ground ice combined with the atmospheric D/H will suggest, whether the ground ice presently is a net receiver or supplier of water to the northern ice cap.

Citation: Fisher, D., R. Novak, and M. J. Mumma (2008), D/H ratio during the northern polar summer and what the Phoenix mission might measure, *J. Geophys. Res.*, *113*, E00A15, doi:10.1029/2007JE002972.

1. Introduction

[2] The purpose of this paper is to lay out what is known about the D/H ratio in the atmosphere during the Phoenix mission and go over the atmospheric processes that will alter the ratio during the mission and to relate the D/H measured for the ground ice to the long-term water cycle and water reservoir sizes. In addition to getting a D/H for the atmospheric water vapor, the Thermal Evolved Gas Analyzer (TEGA) instrument will measure D/H of the samples obtained from the surface, in particular, from the ice-rich layer thought to be only 5 to 10 cm down. The D/H values associated with the upper centimeter of this "ice table" should relate to some average D/H of the ice cap and the deeper ground ice and to the recent net mass balance of the ice table. Interpretive possibilities are touched on.

[3] The primary D/H data are from *Mumma et al.* [2003] and *Novak et al.* [2005, 2007], which are presented in Figure 1a plotted against Pr, the column height of water in microns of H_2O. Figure 1b shows their data at various times during the Mars year as a function of geographic latitude. The D/H data here are always reported relative to its standard terrestrial (Standard Mean Ocean Water, SMOW) ratio of D/H = 1.55×10^{-4}, and the ratio is between number concentrations of the two species. Another way of presenting stable isotope ratios used typically in terrestrial studies is the dimensionless δ(D). It is defined as $\delta(\mathrm{D}) = 1000([\mathrm{D/H}]_{\mathrm{sample}} - [\mathrm{D/H}]_{\mathrm{SMOW}})/[\mathrm{D/H}]_{\mathrm{SMOW}}$, and the units are parts per thousand 0/00. The relative D/H measure is used mostly herein, but in Figure 1a both units are shown for comparison.

[4] Until the *Mumma et al.* [2003] and *Novak et al.* [2005, 2007] work, it was assumed that atmospheric Martian water vapor D/H had a single value around 5.5. They showed otherwise and measured D/H 's between 2.3 and 10 depending on season and latitude. The range of values expected for the Phoenix mission landing site and operational window is marked in Figures 1 and 2.

[5] When water vapor condenses, there can be a change in the D/H ratio of the remaining vapor, with the surface

[1]Glaciology Section, Geological Survey of Canada, Ottawa Ontario, Canada.
[2]Department of Physics, Iona College, New Rochelle, New York, USA.
[3]Planetary and Astrophysical Sciences, Laboratory for Extraterrestrial Physics, NASA Goddard Space Flight Center, Greenbelt, Maryland, USA.

Copyright 2008 by the American Geophysical Union.
0148-0227/08/2007JE002972

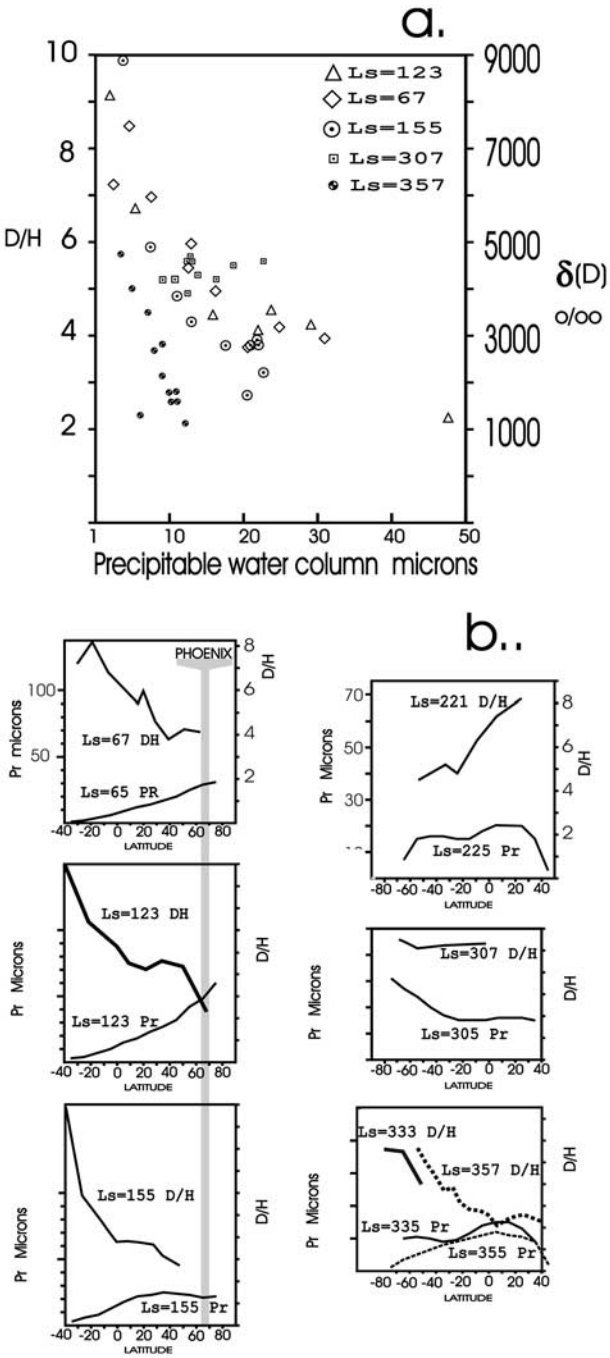

Figure 1. (a) *Mumma et al.* [2003] D/H data plotted against the TES derived Pr measurements. (b) The same (D/H) and Pr data plotted with respect to latitude for various Ls. The Phoenix landing zone latitude strip is marked. Within this strip the expected atmospheric minimum (D/H) ~2 occurs when the water column Pr is at its maximum >50 μm.

deposits possibly taking a higher proportion of D with it when it solidifies out of the atmosphere. This phase change fractionation alters D/H in a way that depends on the manner in which the vapor is removed and on the amount and seasonal evolution of the ice cloud amount. The basic theory of this mixed fractionation process is used to establish the range of D/H that it allows. The *Mumma et al.* [2003] and *Novak et al.* [2005, 2007] (hereinafter referred to as Mumma-Novak) results are compared to the predictions that follow from the simple mixed fractionation theory. It is concluded that phase change fractionation alone cannot explain the seasonal D/H cycle.

[6] The extra concept suggested by *Fisher* [2007] is that different ice reservoirs each have a unique average D/H depending on their size, accessibility, and location. The seasonal atmospheric D/H at a given location is largely determined by the reservoirs' D/H once its water has made it into the atmosphere. The northern ice cap and the subsurface ground ice reservoirs are the dominant sources and probably drive the polar D/H observed during the summer and early fall. Once these sources' water has been cold trapped back to the surface in the late fall, what is left is probably from smaller more southerly reservoirs. These scenarios [*Fisher*, 2007] are discussed.

[7] The Phoenix mission will land in the middle of the polar ground ice zone and be able to measure the amount and D/H of the early summer's water vapor as well as sample and measure the ground ice's D/H. The atmospheric water vapor will come from the ice cap and from the ground ice in various proportions during the mission and further be altered by phase change fractionation and by changes in ice cloudiness during the mission. The Phoenix will have the chance to measure most aspects of all these drivers and see how the D/H is affected. Such a suite of data will cast considerable light on the dominant processes and fluxes moving water around in the polar regions.

[8] A detailed description of the spectral methods used to get HDO concentrations in Mars' atmosphere are given in Appendix A.

2. Seasonal D/H Data

[9] The first impression from Figure 1a is that the atmospheric water vapor D/H is very large when the atmosphere's water vapor column, Pr, is small. The Mumma-Novak data are represented in Figure 1b as functions of latitude and Ls along with the Mars Global Surveyor (MGS) Thermal Emission Spectrometer (TES) evaluations of seasonal water column height from *Smith* [2002]. The Phoenix landing zone (65–70°N) is shaded, and one can see in the middle (Ls ~ 115) of the Phoenix time window that the expected air D/H should be ~2. However, the Pr for this measure was ~49 μm. One can speculate that over polar cap itself, when Pr $\geq$ 80 μm (at Ls ~ 115), D/H could be even smaller. Figure 2a shows Pr and D/H versus Ls for three latitude bins. For the "polar bin" (60°–90°N latitude) the *Smith* [2002] TES data have a max Pr of 70 μm. Earlier Mars Atmospheric Water Detector (MAWD) data from the Viking era give a slightly higher maximum [*Haberle and Jakosky*, 1990], and they likely vary from year to year. Figure 2a shows the approximate Phoenix 90 sol mission window 75 < Ls < 125 in light shading and a 30 sol extension in darker shading. The black dots and dashed lines give D/H data points derived by averaging the Mumma-Novak data in the indicated latitude bins. One can see that the water vapor content, Pr shown as

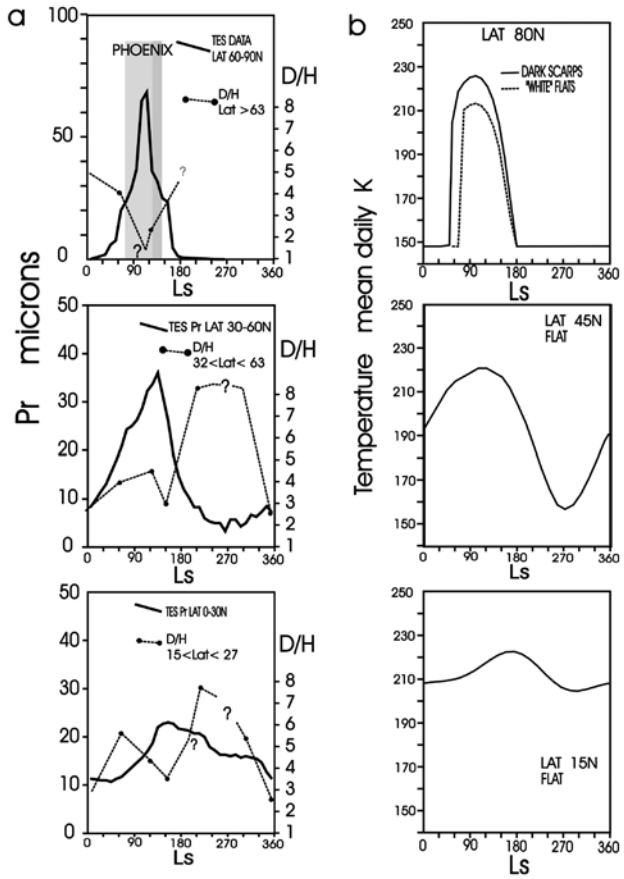

Figure 2. (a) The (D/H) and Pr data (as in Figure 1) versus Ls plotted in three latitude bins. The nominal Phoenix landed window (75 < Ls < 142) and its 30 sol extension are shown shaded. The precipitable water vapor Pr maximizes and (D/H) minimizes at the same time, very close to the Ls of maximum surface temperature from Figure 2b. Temperature itself seems to provide the driver for the seasonal Pr "wave." (b) Surface temperatures for three latitude zones calculated using a simple energy balance model and a coupled subsurface conductivity model. The temperature model is a simple energy balance model with no advection of air but with subsurface conduction. The temperatures presented are typical of others [see, e.g., *Jakosky*, 1983].

solid lines, tends to be in antiphase with the D/H. This is especially true of the polar region.

[10] In the nonpolar zones, 30–60°N and 0–30°N, there are secondary D/H minima (Figure 2a). The secondary minimum for the 30–60°N zone occurs well into the rising surface temperature trend, when the buried water reservoirs would start to be reintroduced to the atmosphere. The secondary minimum for the 0–30°N band could be due to cross equator mixing from the southern late summer hot season.

[11] There is a strong tendency for the D/H to be larger in the southern hemisphere (Figure 1b). This is likely because there are larger more accessible subsurface reservoirs in the north and the southern ice cap is not presently exposed to summer water sublimation as is the north cap. The "ice caps" are hypothesized to have a relatively low average D/H ratio and thus serve in the northern hemisphere as the largest source of "low D/H" water vapor in the northern summer [*Fisher*, 2007]. The hemispheric trend also suggests that the effective inter zonal mixing time for water vapor must be rather long [*Fisher*, 2007].

[12] The northern ice cap is certainly the largest single source of water vapor during the Mars spring and summer, but *Boynton et al.* [2002] have demonstrated that there are massive ground ice reservoirs within a few centimeters of the surface at high polar latitudes, poleward of 60 degrees. The ice cap and the ground ice reservoirs get activated almost as soon as the CO_2 snow/frost has departed at any given latitude in the spring. At the high latitudes the regolith cover is so thin its adsorbed water contribution to the growing spring water dome cannot be very extensive. For the polar region, the compound "frost" CO_2 + dust + H_2O can only be a minor source of water vapor. This can be inferred from the *Smith* [2002] Pr seasonal data that show that virtually all the polar water vapor is removed before the compound "frost" begins to thicken [*Zuber et al.*, 1998]. Transferring the water vapor into polar ice clouds remains a possible means of cycling the water vapor as does direct deposition to the surface of the ice cap and onto and into the polar regolith especially onto cold spots in the shade. Combinations of these possible processes are taken up and examined in section 3.

[13] Equatorward of 60 degrees any ice table is protected by thicker protective regolith, which takes longer for the summer warm wave to penetrate. Until the summer warming wave reaches a buried reservoir, it cannot act as a source although the adsorbed water in the regolith can act as one. Tropical seasonal water might be confined only to adsorbed water, because any ice table is just too deep for the depth decaying summer temperature wave to activate it [e.g., *Zent et al.*, 1986]. Figure 2b shows model-produced daily mean temperature in north latitude bands. The temperature and water vapor, Pr, versus Ls (Figure 2a) are in phase, suggesting that the main driver for the air water vapor, Pr, is the near surface temperature. As an aside, it appears that presently the main driver of non-ice cap water vapor is simply the near surface temperature. It follows that no substantial southward migration of polar water is necessary to explain the Pr seasonal cycle. There may be out migration of polar water, but the apparent "wave" in Pr from the pole can mostly be driven by local temperature and is not necessarily an indicator of migration by itself.

3. Theoretical Discussion of Seasonal D/H

[14] As the spring and summer warm season develop at a given latitude, the local water reservoirs begin to get activated and give off water to the atmosphere, with some delay dependent on when the warming temperature reaches the water resource. For the high-latitude ground ice and the ice cap this begins as soon as the solid CO_2 is gone because the water ice is either at the surface in the case of the ice cap or within centimeters of the surface in the case of the polar ground ice. As the water of a given reservoir (latitude) is introduced to the atmosphere and the water content at that latitude grows, the D/H there reflects the D/H of the ice reservoir mixed with some amount of other latitude's adsorbed water. To a first approximation (given the weak

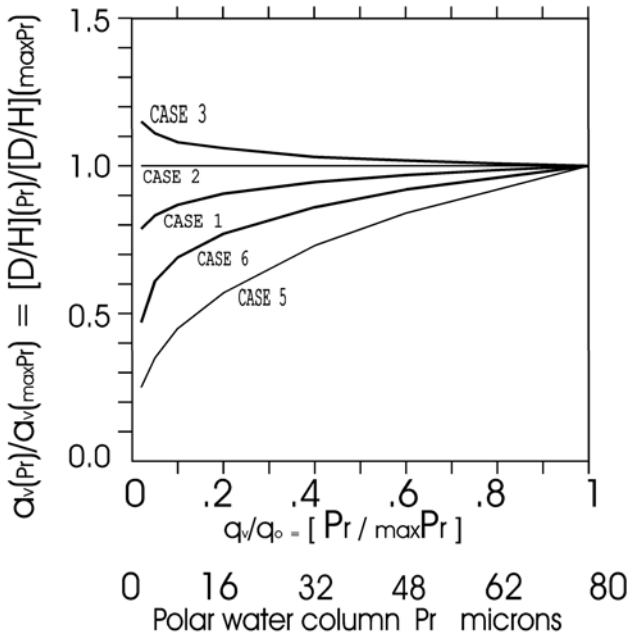

Figure 3. The fractionation model results show that under all but one case, the modeled atmospheric D/H should stay the same or get smaller as Pr decreases into the fall. This is contrary to the Mumma-Novak data set presented in Figures 1 and 2. The one example (case 3) shows a modest increase in D/H as Pr decreases, and this is due to the presence of ice clouds.

nature of interlatitude mixing), at the maximum Pr, the atmospheric D/H reflects that latitudes water reservoir value [*Fisher*, 2007].Also given that the adsorbed water will have the highest D/H, the lowest atmospheric Pr will coincide with the highest D/H [*Fisher*, 2007]. Over the ice cap itself the situation might be more complex with the dark scarps providing water vapor with the cap's D/H average that is then partly removed over the "white" colder accumulation regions. The amount of sublimation, vertical mixing and the removal rates should be carefully modeled especially in the lead up to the summer maximum in water vapor. But that is beyond the scope of this paper.

[15] During the collapse of the water vapor dome in the Martian fall there might be some fractionation of the water vapor left in the air. The extreme case for fractionation would be approximated by Rayleigh fractionation from a vapor mass that loses ice crystals as soon as they form ("precipitation"), i.e., an open cloud system. This process has been extensively studied in models [*Montmessin et al.*, 2005; *Fouchet and Lellouch*, 2000]. The evolution of the collapsing water vapor mass D/H ratio would then follow [*Dansgaard*, 1961]:

$$a_v(t) = a_v(0)\left(\frac{q_v(t)}{q_v(0)}\right)^{(\acute{a}-1)} \tag{1}$$

where $a_v(t)$ = [HDO]/(2[H_2O]) is the D/H number ratio at time t counted from the instant of the maximum (e.g., Ls = ~115 for the N pole) when a_v (0) is equal to the minimum D/H (~2); q_v is the total H content in [number of H atoms/ cm^2] in the vertically integrated water column. It is assumed that the column is well mixed. The fractionation coefficient α for any point during the collapse is

$$\alpha = \frac{\left(\frac{\mathrm{HDO}}{\mathrm{H_2O}}\right)_{\mathrm{instantaneous-vapor}}}{\left(\frac{\mathrm{HDO}}{\mathrm{H_2O}}\right)_{\mathrm{instantaneous-new\ ice}}}$$

The solid to vapor α for terrestrial temperatures is given by *Majoube* [1971] and *Merlivat and Nief* [1967], but since their experimental range was far outside the Mars range of polar temperatures, an average value for α will be taken to be 1.35 [see, e.g., *Yung et al.*, 1988]. Equation (1) produces the maximum possible reduction in atmospheric D/H, when the water vapor dome collapses. In equation (1) $q_v(t)/q_v(0)$ can be given by Pr(t)/max Pr. For example if (Pr(t)/max Pr) is 0.2 and a_v (0) = 2 then a_v (t)/a_v (0) is 0.57 and vapor would have a D/H of ~1, which immediately can be seem to contradict the observations (see Figure 2a). The assumptions of an open cloud system with complete removal of vapor condensed in the atmosphere implies that clouds and precipitation are the dominant means of removal or water vapor during the end of summer collapse.

[16] Using the approach laid out by *Fisher* [2007], the equation (1) model can be extended to include some mixed removal processes. Assume that there are suspended ice clouds that have some prescribed constant fraction f of atmospheric water vapor and whose ice crystals are in isotopic equilibrium with the ambient water vapor (α = 1.35). Assume also that there is some direct deposition onto the surface of the ice cap or into the ground ice/regolith that would take out all the vapor and essentially do so with no fractionation, i.e., α = 1.0. There are researchers who have thought this is the dominant means of removal of water vapor from the Martian air [e.g., *McElroy and Yung*, 1976; *Jakosky*, 1991], and there is some merit in their view, because it is unlikely that precipitation plays much of a role in accumulation. Finally, assume there is some ice deposited on the surface, which is in isotopic equilibrium with a well mixed atmospheric vapor reservoir (with α = 1.35). This could be done if there was precipitation from the ice clouds or as frost on the surface if the water vapor was very well mixed on relatively short scale times. If the surface accumulations by direct deposit (with α = 1) and by equilibrium frosting and precipitation (with α = 1.35) have proportions w_s and w_p, respectively, then equation (1) is amended to

$$\frac{a_v(t)}{a_v(0)} = \left(\frac{q_v(t)}{q_v(0)}\right)^{\left(w_s + w_p\acute{a} - 1 - \phi(\acute{a} - \omega_\sigma - \omega_\pi\acute{a})\right)/1+\phi\acute{a}} \tag{2}$$

If w_s = 0, w_p = 1, and f = 0, then equation (2) would become equation (1). Having w_s = 0, w_p = 1, α = 1.35 models the case for an open cloud precipitating system and/or a well mixed water vapor column with equilibrium between the remaining vapor and the surface deposit. Having w_s = 1, w_p = 0, α = 1.0 models the case for very slow vertical mixing and complete cold trap removal of water once it gets close to the surface. The truth has to lie between the two cases so various cases are defined in Table 1 and shown in Figure 3. Figure 3 shows the evolution of $a_v(t)/a_v(0)$ as a function of

Table 1. Mixed Modes of Accumulation

	Comment	w_s	w_p	f
Case 1	mixed open cloud and direct deposition	0.75	0.25	0.1
Case 2	pure direct deposition	1	0	0
Case 3	only direct deposition with some clouds	1	0	0.1
Case 5	pure open cloud precipitation with clouds	0	1	0.1
Case 6	mixed open cloud and direct deposition	0.5	0.5	0.1

$q_v(t)/q_v(0)$ using equation (2) for various "cloud" cases listed in Table 1. The water vapor content ratio $q_v(t)/q_v(0)$ quite sensibly can be taken equal to the ratio of precipitable water Pr(Ls) to the maximum value at Ls = 115; i.e., $q_v(t)/q_v(0)$ = Pr(Ls)/Pr(115).

[17] Only case 3 in Table 1 results in a modest increase in D/H as fall approaches (Figure 3). This case requires the combination of ice cloud at 10% of the vapor mass and removal at the surface by only direct deposition. Since the D/H data show a substantial increase after the summer peak warmth this simple Rayleigh-type mixed model by itself does not seem to be adequate.

4. Multiple Reservoirs, Seasonal D/H, and Phoenix

[18] From model considerations, it has been suggested that the average D/H for various water reservoirs at various latitudes depends on the size and accessibility of the reservoir [*Fisher*, 2007]. The model considers two coupled reservoirs that lose and gain mass on seasonal, obliquity and secular timescales. The main reservoirs are the north ice cap and the ring of near-surface ground ice that surrounds it [*Boynton et al.*, 2002]. Other smaller reservoirs are the adsorbed water in the upper regolith and possibly the seasonal ice clouds of the polar hood.

[19] Figure 2a shows that the seasonal minima for the polar, midlatitude and tropical atmospheric water vapor D/H, coincide with the maximum Pr. These minima are taken as the hypothetical D/H averages for the latitude's main reservoirs. These zonal minima appear in Figure 4a. Also the line in Figure 4b is the *Fisher* [2007] modeled average (D/H) for an ice cap coupled to other reservoirs of various sizes (assuming the water all started out at D/H = 1 3 $\times$ 10^9 years ago). The shaded block shows the probable range for the ice cap average D/H using the Mumma-Novak results extrapolated to a Pr of 80 μm. The heavy arrow shows the model predicted extreme case that assumes there is a ground ice reservoir 10 times bigger than the ice cap's mass that is accessible to atmospheric processes and exchanging water with the ice cap. The secondary minima in the equatorial zones are indicated by the lighter shading. These secondary minima in D/H that do not coincide with the maximum in Pr could be there, because even though the water vapor flux out of the regolith is still small at that part of the year, it is still upward and comes from the buried reservoir. The lowest values of D/H in the equatorial zone 0–30°N is 2.2 at Ls = 357, which possibly suggests that the equatorial reservoir might be coupled to deep large reservoir [*Fisher*, 2007]. If the low D/H of vapor over the northern ice cap is verified to be 2, then one would be drawn to the conclusion

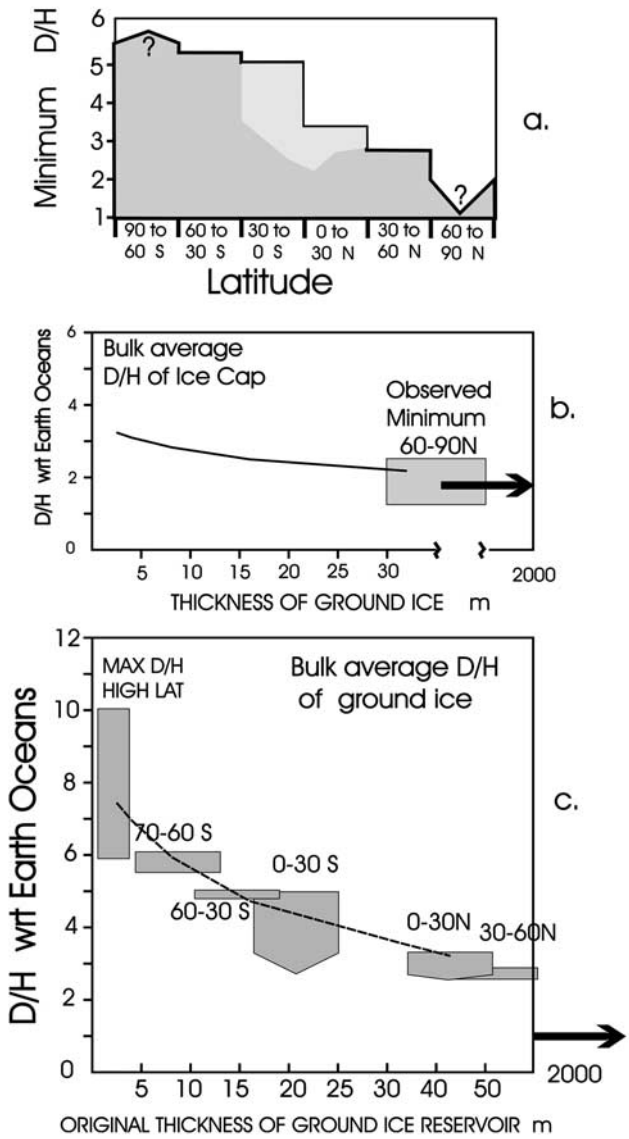

Figure 4. (a) Zonal average atmospheric water vapor D/H for maximum Pr within that zone. The light shading indicates the range of the secondary minima in some nonpolar zones. The most northern measures for minimum D/H refer to latitude 65°N so the north polar cap minimum is indicated as probably lower than that measured value (see Figure 1). Similarly, the D/H minimum south of 70 S can only be extrapolated as larger than measured values for latitude 70°S at Ls = 307. (b) D/H for the northern ice cap predicted from a model [*Fisher*, 2007] and the lowest Mumma-Novak high-latitude D/H and its extrapolation to Pr $\sim$ 80 μm (shaded box). The *x* axis is the thickness of the massive ground ice that is numerically coupled to the ice cap. (c) The modeled [*Fisher*, 2007] average D/H of buried reservoirs as a function of their size. The shaded blocks are the measured seasonal minima from Figure 2. The big horizontal arrows in Figures 4b and 4c are model average D/H if the buried reservoir is 10 times larger than the present northern ice cap. The very low (D/H $\sim$ 2.3) secondary minima in lower latitudes might indicate deeper water from a very large reservoir.

that there is a deep accessible reservoir at least 10 times the size of the ice cap in volume.

[20] Interhemispheric mixing across the equator is also possibly involved in the secondary minima at low latitudes as could some Rayleigh condensation. Of course, more data in and around Ls 270 would greatly help in resolving these possibilities [*Novak et al.*, 2007] as would improved geographic resolution.

[21] Figure 4c shows the modeled average D/H for ground ice reservoirs as a function of their size along with the Mumma-Novak derived zonal minima (the shaded blocks) from Figure 2a. Each latitude bin's minimum has simply been moved over to the theoretical line from [*Fisher*, 2007], which suggests, in that model space, the size of the reservoir in question. It should be remembered that the model predictions are based on a relatively simple model with what are deemed to be the most likely input parameters (MEDIUM case [*Fisher*, 2007]).

[22] The southern hemisphere's tendency toward larger D/H [*Novak et al.*, 2007] is made very clear in Figure 4a, suggesting smaller and/or less accessible water reservoirs in the south. In particular, the combined effect of the permanent CO_2 surface layer and dirt lag on the southern ice cap has largely isolated that cap's water from the atmosphere. One can only speculate on the average D/H of the south caps water ice that presently lies protected under the CO_2 and dirt lag.

5. What Phoenix Will Add

[23] Phoenix (at latitude 68°N) will measure D/H of the atmospheric water soon after landing (Ls $\sim$ 80), The TEGA instrument can provide atmospheric D/H values good to about 30% for mixing ratios (g water vapor/g CO_2) greater than 123 ppm (W. V. Boynton *et al.*, The Thermal and Evolved Gas Analyzer on the Phoenix Mars Lander, manuscript in preparation, 2008). Since the mixing ratio near the beginning of the mission will be about 450 $\pm$ 170 ppm, a useful measure of D/H should be obtained for the surficial air during the day. If plans for a nighttime air sampling succeed there could also be a night D/H. This might reflect the effects of night fogs and frost formation on the effective value of α. The measured D/H will of course relate to the lowest meter of the atmosphere.

[24] The Robot Arm (RA)/ice rasp system will be providing ice samples to TEGA from the top 1 cm of the ice table that is thought to be between 5 and 10 cm below the surface [*Mellon et al.*, 2008] at the landing site. For these much larger ground ice samples TEGA will be determining D/H to better than 5% (W. V. Boynton et al., manuscript in preparation, 2008). This "top-of-ice-table" D/H ratio will represent only the upper layer of a stratified sequence of D/H. If the maximum rate of resurfacing of the ice table is scaled to the maximum Pr at latitude 68 ($\sim$50 μm of water), then the 1 vertical cm sample would represent a substantial 400 years. Of course since the landing site is in patterned terrain formed by thermal cracking of the buried ice, there are likely horizontal variations in the depth to the ice table and possibly of its D/H ratio. There is also the real possibility that thermal cracking at many scales will have mixed deeper water into the uppermost 1 cm by diffusion [*Fisher*, 2005]. TEGA's measures of D/H will be the first direct measure from any buried ice on Mars and should hint, if the ice table here is presently growing at the expense of the ice cap.

[25] In addition to the TEGA provided D/H ratios the Phoenix instrument suite will give essential measurements for accessing and calibrating the models used to interpret the D/H ratios. The MET instrument will provide continuous temperatures and pressures throughout the mission [*Taylor et al.*, 2008] as well as day and night LIDAR measures of cloudiness (dust and ice crystals) up to a maximum height of 20 km [*Whiteway et al.*, 2008]. The SSI camera [*Taylor et al.*, 2008; M. T. Lemmon et al., The Phoenix surface stereo imager investigation, manuscript in preparation, 2008] will provide total water column measures on a regular basis in the day (and hopefully at low Sun). The SSI will also monitor wind by observing the wind indicating Telltale and look for ground frosts and fogs in the morning. The TECP instrument, which is part of the MECA suite will used to measure near surface absolute humidity on a regular basis during the day (and hopefully at low Sun) (A. Zent and S. Wood, TECP and humidity, manuscript in preparation, 2008). With estimates of the diurnal cycles of temperature, humidity and wind over the whole mission there is chance of determining the direction of the net mass balance of the ground ice. This direction would be a help in interpreting the D/H ratio for the ground ice and it relation to the ice cap.

[26] Phoenix will provide important new constraints on the sizes of Mars' water reservoirs and how accessible they are to the surface.

Appendix A: Spectral Methods Used to Get HDO Concentrations in Mars' Atmosphere

[27] Observations were made using the cryogenic echelle spectrometer (CSHELL) at the NASA Infrared Telescope Facility on Mauna Kea, Hawaii [*Tokunaga et al.*, 1990; *Greene et al.*, 1993]. CSHELL has a 256 $\times$ 256 pixel InSb array detector with pixel size of 0.2 arc sec and provides spatial coverage along the 30 arc sec long slit. The slit was oriented north-south on Mars along the central meridian. The 0.5 arc sec wide slit (resolving power, = $\nu/\Delta\nu \sim 4 \times 10^4$) was used for the Mars observations. The slit width defines the spectral resolving power, but the spatial resolution on the planet also depends on the image quality during the observation. Measuring the point spread function of a star (typically, full width at half maximum $\sim$0.6–1.0 arc sec) provides a measure of the spatial resolution on the disk of Mars.

[28] Spectra were acquired using a sequence of four scans (source, sky, sky, source) with an integration time of 2 min on source per sequence of scans. Sky spectra were obtained by nodding the telescope away from Mars providing sky cancellation via pixel-by-pixel subtraction (Mars-sky-sky + Mars). Flat-field and dark frames were obtained immediately following each scan sequence. Spectra of an infrared standard star were obtained at the same grating settings through a 4 arc sec wide slit for absolute flux calibration of the spectra and determination of the seeing through the Earth's atmosphere. Spectra of the star are also taken using a 0.5 arc sec slit; these spectra are useful in building a model of the Earth's atmosphere. Images of Mars at 3.5 μm were

taken before and after each sequence of scans to assess drift and to update telescope tracking rates as needed.

[29] The data were processed using algorithms specifically tailored to our CSHELL observations [*DiSanti et al.*, 2001, *Novak et al.*, 2002]. Initial data processing includes flat fielding, removal of high dark current pixels and cosmic ray hits, and registration of spectral frames such that the spectral dimension falls along a row and the spatial dimension is orthogonal to this. After sky subtraction, the resulting frame is analyzed to determine the column density of gases in Mars' atmosphere. Spectral extracts were taken by summing groups of three rows (0.6 arc sec) on the chip; a relative velocity of at least 12 km s^{-1} creates a Doppler shift of Mars' spectrum with respect to that of Earth. A spectral model of Earth's atmosphere is constructed to match the observed spectrum; this model is then subtracted from the observed spectrum to isolate weak solar Fraunhofer lines and absorption lines from Mars' atmosphere. The continuum in the observed spectrum is created by both reflected sunlight from the surface of Mars and thermal emission from Mars' surface and atmosphere. As the thermal emission increases, the observed equivalent width of the solar Fraunhofer lines decrease. The model used to determine the column density of gases in the retrieved Mars spectrum includes the solar spectrum from the ATMOS database [*Geller*, 1992], a two-way transmittance and radiance model of Mars' atmosphere, and thermal emission from Mars' surface and atmosphere. Originally, the Spectrum Synthesis Program (SSP) [*Kunde and Maguire*, 1974] was used to construct the atmospheric models; since 2006, *Edwards* [1992] has been used to construct the models. Both models use the HITRAN database [*Rothman et al.*, 2005].

References

Boynton, W. V., et al. (2002), Distribution of hydrogen in the near surface of Mars: Evidence for subsurface ice deposits, *Science*, *297*, 81–85, doi:10.1126/science.1073722.

Dansgaard, W. (1961), The isotopic composition of natural waters, *Medd. Groenland*, *165*(2), 120 pp.

DiSanti, M. A., M. J. Mumma, N. Dello Russo, and K. Magee-Sauer (2001), Carbon monoxide production and excitation in Comet C/1995 O1(Hale-Bopp): Isolation of native and distributed CO sources, *Icarus*, *153*, 361–390, doi:10.1006/icar.2001.6695.

Edwards, D. P. (1992), GENLN2: A general line-by-line atmospheric transmittance and radiance model, version 3.0 description and users guide, *Tech. Note NCAR/TN-367-STR*, Natl. Cent. for Atmos. Res., Boulder, Colo.

Fisher, D. A. (2005), A process to make massive ice in the Martian regolith using long-term diffusion and thermal cracking, *Icarus*, *179*, 387–397, doi:10.1016/j.icarus.2005.07.024.

Fisher, D. A. (2007), Mars' water isotope (D/H) history in the strata of the north polar cap: Inferences about the water cycle, *Icarus*, *187*, 430–441, doi:10.1016/j.icarus.2006.10.032.

Fouchet, T., and E. Lellouch (2000), Vapour pressure isotope fractionation effects in planetary atmospheres: Application to deuterium, *Icarus*, *144*, 114–123, doi:10.1006/icar.1999.6264.

Greene, T. P., A. T. Tokunaga, D. W. Toomey, and J. B. Carr (1993), CSHELL: A high spectral resolution 1–5 μm cryogenic echelle spectrograph for the IRTF, *Proc. SPIE*, *1946*, 313–324, doi:10.1117/12.158684.

Haberle, R. M., and B. M. Jakosky (1990), Sublimation and transport of water from the north residual polar cap on Mars, *J. Geophys. Res.*, *95*, 1423–1437, doi:10.1029/JB095iB02p01423.

Jakosky, B. M. (1983), The role of seasonal reservoirs in the Mars water cycle: 1. Seasonal exchange of water with the regolith, *Icarus*, *55*, 1–18, doi:10.1016/0019-1035(83)90046-5.

Jakosky, B. M. (1991), Mars volatile evolution: Evidence from stable isotopes, *Icarus*, *94*, 14–31, doi:10.1016/0019-1035(91)90138-J.

Kunde, V. G., and W. C. Maguire (1974), Direct integration transmission model, *J. Quant. Spectrosc. Radiat. Transf.*, *14*, 803–817, doi:10.1016/0022-4073(74)90124-1.

Majoube, M. (1971), Fractionnement en oxygè 18 et en deutérium entre l'eau et sa vapeur, *J. Chem. Phys.*, *10*, 1473.

McElroy, M. B., and Y. L. Yung (1976), Oxygen isotopes in the Martian atmosphere: Implications for the evolution of volatiles, *Planet. Space Sci.*, *24*, 1107–1113, doi:10.1016/0032-0633(76)90148-3.

Mellon, M. T., W. V. Boynton, W. C. Feldman, R. E. D. Arvidson, T. N. Titus, J. L. Bandfield, N. Putzig, and H. Sizemore (2008), A prelanding assessment of the ice table depth and ground ice characteristics in Martian permafrost at the Phoenix landing site, *J. Geophys. Res.*, doi:10.1029/2007JE003067, in press.

Merlivat, L., and G. Nief (1967), Fractionnement isotopique lors des changements d'état solide-vapeur et liquide-vapeur de l'eau à des températures inférieures à 0°C, *Tellus*, *19*, 122–127.

Montmessin, F., T. Fouchet, and F. Forget (2005), Modeling the annual cycle of HDO in the Martian atmosphere, *J. Geophys. Res.*, *110*, E03006, doi:10.1029/2004JE002357.

Mumma, M. J., R. E. Novak, M. A. DiSanti, B. Bonev, N. Dello Russo, and K. Magee-Sauer (2003), Seasonal mapping of HDO and H_2O, in *Sixth International Conference on Mars Atmosphere*, Abstract 3186, Jet Propul. Lab., Pasadena, Calif.

Novak, R. E., M. J. Mumma, M. A. DiSanti, N. Dello Russo, and K. Magee-Sauer (2002), Mapping of ozone and water in the atmosphere of Mars near the 1997 aphelion, *Icarus*, *158*, 14–23, doi:10.1006/icar.2002.6863.

Novak, R. E., M. J. Mumma, S. Lee, L. Ivanov, B. Bonev, and G. Villanueva (2005), Mapping of D/H and ozone in the Martian atmosphere near perihelion, *Bull. Am. Astron. Soc.*, *35*(3), 669.

Novak, R. E., M. J. Mumma, G. Villanueva, B. Bonev, and M. DiSanti (2007), Mapping of HDO and H_2O in the Martian atmosphere, in *Seventh International Conference on Mars*, Jet Propul. Lab., Pasadena, Calif.

Rothman, L. S., et al. (2005), The HITRAN 2004 molecular spectroscopic database, *J. Quant. Spectrosc. Radiat. Transf.*, *96*, 139–204, doi:10.1016/j.jqsrt.2004.10.008.

Smith, M. D. (2002), The annual cycle of water vapor on Mars as observed by the Thermal Emission Spectrometer, *J. Geophys. Res.*, *107*(E11), 5115, doi:10.1029/2001JE001522.

Taylor, P. A., D. C. Catling, M. Daly, C. S. Dickinson, H. P. Gunnlaugsson, A. Harri, and C. F. Lange (2008), Temperature, pressure, and wind instrumentation in the Phoenix meteorological package, *J. Geophys. Res.*, *113*, E00A10, doi:10.1029/2007JE003015.

Tokunaga, A. T., D. W. Toomey, J. Carr, D. N. B. Hall, and H. W. Epps (1990), Design for a 1–5-μm cryogenic echelle spectrograph for the NASA IRTF, *Proc. SPIE*, *1235*, 131–143, doi:10.1117/12.19082.

Whiteway, J., M. Daly, A. Carswell, T. Duck, C. Dickinson, L. Komguem, and C. Cook (2008), Lidar on the Phoenix mission to Mars, *J. Geophys. Res.*, *113*, E00A08, doi:10.1029/2007JE003002.

Yung, Y. L., J. Wen, J. P. Pinto, M. Allen, K. K. Pierce, and S. Paulson (1988), HDO in Martian atmosphere: Implications for the abundance of crustal waters, *Icarus*, *76*, 146–159, doi:10.1016/0019-1035(88)90147-9.

Zent, A. P., F. P. Fanal, J. R. Salvail, and S. E. Postauko (1986), Distribution and state of H2O in the high-latitude shallow subsurface of Mars, *Icarus*, *67*, 16–36.

Zuber, M. T., et al. (1998), Observations of the north polar region of Mars from the Mars Orbital Laser Altimeter, *Science*, *282*, 2053–2060, doi:10.1126/science.282.5396.2053.

D. Fisher, Glaciology Section, Geological Survey of Canada, NRCan, 601 Booth Street, Ottawa ON, K1A 0E8, Canada. (david.fisher@nrcan.gc.ca)

M. J. Mumma, Planetary and Astrophysical Sciences, Laboratory for Extraterrestrial Physics, NASA Goddard Space Flight Center, Greenbelt, MD 20771, USA. (mmumma@lepvax.gsfc.nasa.gov)

R. Novak, Department of Physics, Iona College, 715 North Avenue, New Rochelle, NY 10801, USA. (rnovak@iona.edu)